A Switching Cascade Sliding PID-PID Controllers Combined with a Feedforward and an MPC for an Actuator in Camless Internal Combustion Engines

Paolo Mercorelli and Nils Werner

Abstract— **This paper deals with a hybrid actuator composed by a piezo part and a hydraulic one and with a cascade PID-PID control structure for camless engine motor applications. The idea is to use the advantages of both, the high precision of the piezo part and the force of the hydraulic one. In fact, piezoelectric actuators (PEAs) are commonly used for precision positionings, despite PEAs present nonlinearities, such as hysteresis, saturations, and creep. In the control problem such nonlinearities must be taken into account. In this paper the Preisach dynamic model with the above mentioned nonlinearities is considered together with a cascade PID-PID controller combined with a feedforward and an Model Predictive Control regulator. The Model Predictive Control uses a particular geometric structure to speed up the dynamic response of the controlled system. In particular, the hysteresis effect is considered and a model with a switching function is used also for the controller design. Simulations with real data are shown.**

Key-words: PID controllers, Lyapunov's approach, piezo actuators, Model Predictive Control

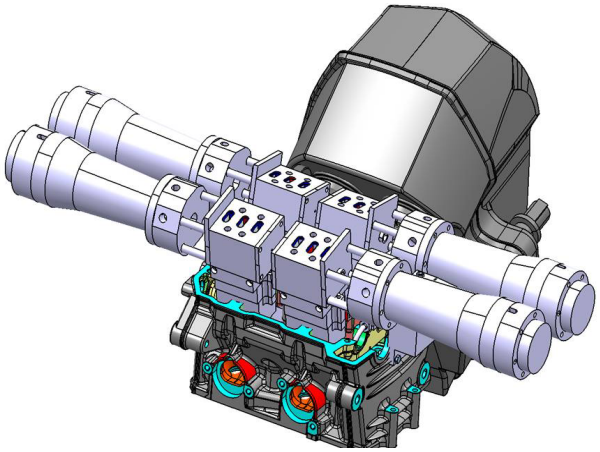

Fig. 1. New structure of the engine.

I. Introduction

In the last few years, variable engine valve control in camless systems has attracted a lot of attention because of its ability to reduce pumping losses (work required to draw air into the cylinder under a part-load operation) and to increase torque performance over a wider rage than conventional spark-ignition engine. Variable valve timing also allows control of internal exhaust gas recirculation, thus improving fuel economy and reducing NOx emissions. Fig. 1 shows the phase diagram of the positions of an engine intake and exhaust valves. In this figure the intake and the exhaust valve position profile are indicated. Figure 1 indicates a possible new engine structure with, evidently, four piezo actuators. Generally speaking, this project closely concerns a new conception of the functionality of some parts of the engine. In particular, a camless engine is proposed. The idea which this paper presents is to use hybrid actuator composed by a piezo part and a hydraulic one in order to take advantages of both: the high precision and velocity of the piezo part and the force of the hydraulic one. Hybrid actuators represent a viable solution to find some compromise for control systems specifications such as precision, velocity and robustness, [1]. Moreover, piezo actuators present in general less problems of electromagnetic compatibility due to the quasi-absence of the inductance effects. The main advantage of PA is nanometer scale, high stiffness, and a fast response. However, since PA has nonlinear property which is called hysteresis effect, it leads to inaccuracy in positioning control with a high precise performance. In this paper the hysteresis effect is a model using a linearization. A linear boundary of the hysteresis is considered and a switching approach is used to follow the hysteresis characteristics. The easiest idea is to consider the upper and the lower bound of the linear characteristic. PID regulators are very often used in industrial applications because of their simple structure, even though in the last years advanced PID controllers have been developed to control nonlinear systems, [2]. Recently, variable engine valve control has attracted a lot of attention because of its ability to improve fuel economy, reduce NOx emissions and to increase torque performance over a wider range than a conventional spark-ignition engine. In combination with a microprocessor control, key functions of the motor management can be efficiently controlled by such mechatronic actuators. For moving distances between 5 and 8 mm, however, there are other actuator types with different advantages. The PID control structure presented in this paper is quite similar to the sliding control structure presented in [3]. Sliding mode structures are often used in actuator control. In fact, in [4] an integral sliding mode controller (is proposed and designed for controlling DC motor in a servo drive. Even though sliding mode approach can generate some chattering problems is this approach very often applied with some variations and in order to overcome this drawback some recent contributions proposed some different schemes, e.g., [5], [6] and [7]. In [8]

Paolo Mercorelli is with the Institute of Product and Process Innovation, Leuphana University of Lueneburg, Volgershall 1, D-21339 Lueneburg, Germany. Tel.: +49-(0)4131-677-5571, Fax: +49-(0)4131-677-5300. mercorelli@uni.leuphana.de. Nils Werner is with the Faculty of Automotive Engineering, Ostfalia University of Applied Sciences, Kleiststr. 14-16, D-38440 Wolfsburg, Germany. Tel. +49-(0)5361-831615 Fax. +49-(0)5361-831602. n.werner@ostfalia.de

the authors presented an adaptive PID controller design for the valve actuator control based on the flatness property and interval polynomials. The objective of this paper is to show:

- A model of the a hybrid actuator
- A PID-PID cascade regulator combined with a feedforward regulator
- An MPC structure using a geometric structure to speed up the dynamic response.

The paper enhances the results presented in [9] and presents a combination of a switching cascade PID-PID structure and feedforward regulators. The feedforward regulator is the same as in [10] in which a combination between a Model Predictive Control (MPC) combined with two feedforward regulators is shown. The advantage of using PID controller is due to their easy practical implementation. Control PID structure is a switching one which considers the proposed switching model of the hysteresis effect in order to eliminate the hysteresis effect on the control output. Hysteresis effects are well known and different proposed compensation schemes are present in practical applications such as that proposed in [11].

In order to speed up the dynamics of the actuator without using strong actions of the regulators which can generate large oscillations and thus tracking errors, a geometric pre-compensator is proposed in connection with MPC. Starting from the contribution presented in [12], in which an MPC algorithm is presented, this paper shows an idea to use a pre-compensator to avoid higher order of controllers. The idea presented is based on a geometric approach as that proposed in [13].

The paper is organized with the following sections. Section II is devoted to the model description. In Section III an algorithm is shown to derive the PID control laws. Section IV presents an MPC approach considering a pre-compensator calculated using a geometric approach. The paper ends with Section V in which simulation results of the proposed valve using real data are presented. After that the conclusions follow.

II. Modeling of the Piezo Hydraulic Actuator

In the diagram of Fig. 3 the T-A connection links the couple of valves with the tank and the P-B connection links the couple of valves with the pump. In the position of Fig. 3 connections T-A and P-B are maximally open and the couple of valves are closed because point B is under pressure. When the piezo acts its force, the mechanical servo valve moves and begins to close these connections. When the mechanical servo valve is in the middle position, both connections (T-A and P-B) are closed and connections A-P and B-T begin to open. At this position also both motor valves begin to open because point A is under pressure. Figure 2 shows in detail a part of the hybrid structure which consists of a piezo actuator combined with a mechanical part. These two parts are connected by a stroke ratio to adapt the stroke length. The proposed nonlinearity model for PEA is quite similar to these presented in [14] and in [15]. It is basically constructed from a sandwich model as shown in Fig. 4, which is based on the following hypothesis. According to the proposed sandwich

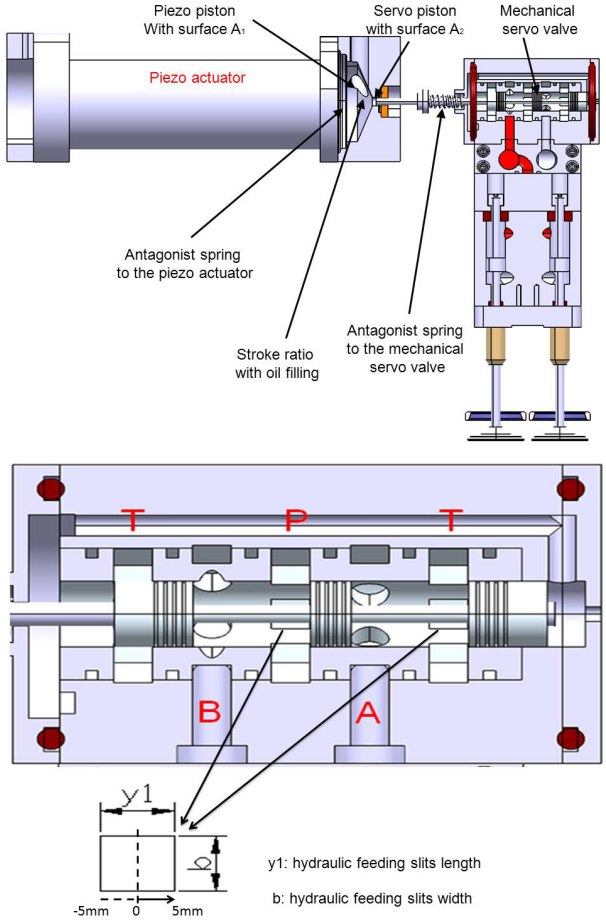

Fig. 2. Structure of the hybrid actuator and detail of the slits

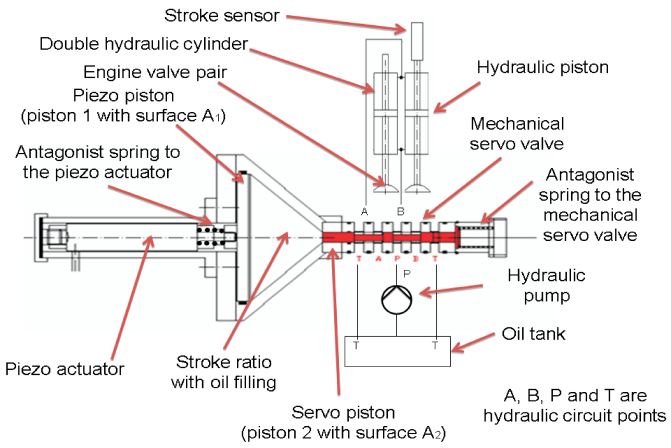

Fig. 3. Scheme of the whole Hybrid Piezo Hydraulic structure

model, a PEA is constituted like a three layer sandwich. The middle layer is the effective piezo layer (P-layer), and the two outside layers connected to the electrodes are known in the literature as interfacing layers (I-layers). The P-layer is the one that has the ordinary characteristics of piezo effects but without the nonlinearities of hysteresis and creep so that its behavior can be modeled by an equivalent linear circuitry. On the contrary, the I-layers do not contribute any piezo effect;

they are just parts of the circuit connecting P-layer to the electrodes in series. In [15] it is hypothesized that each of

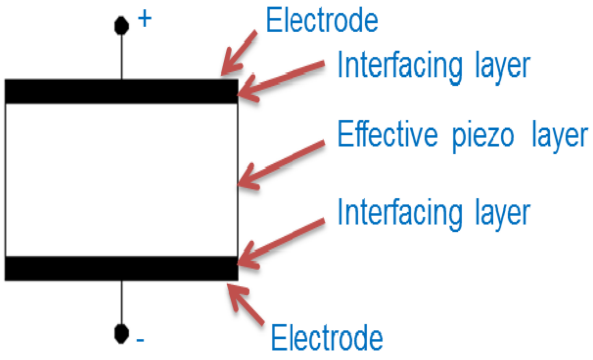

Fig. 4. The sandwich model of the PEA

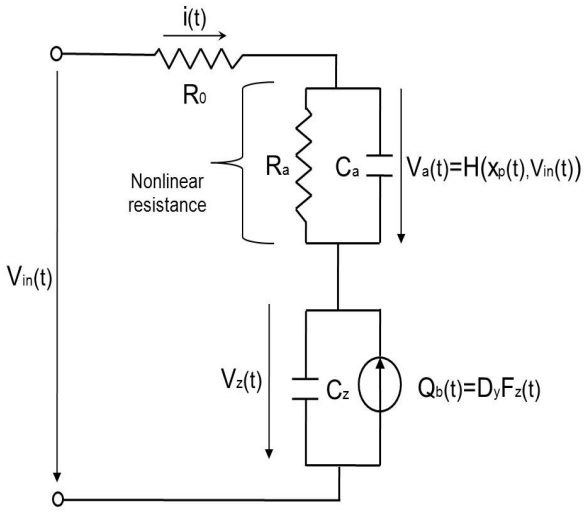

Fig. 5. Electrical part of the model

the I-layers can be equivalently represented by a capacitor and a resistor connected together in parallel. Together with the equivalent circuitry for P-layer, Fig. 5 shows the equivalent circuitry for a PEA with the I-layer nonlinearities of hysteresis and creep, in which two I-layers are combined together as C_a and R_a. The I-layer capacitor, C_a, is an ordinary capacitor, "which might be varied slightly with some factors, but here it would be assumed constant first for simplicity. The I-layer resistor, R_a , however, is really an extraordinary one with a significant nonlinearity. The resistance is either fairly large, say $R_a > 10^6\ \Omega$, when the voltage $\|V_a\| < V_h$, or is fairly small, say $R_a < 1000$, when $\|V_a\| > V_h$. In [15], the threshold voltage, V_h, is defined as the hysteresis voltage of a PEA. The authors in [15] gave this definition due to the observation that there is a significant difference and an abrupt change in resistance across this threshold voltage and it is this resistance difference and change across V_h that introduce the nonlinearities of hysteresis and creep in a PEA. The hysteresis effect could be seen as a function of input $V_{in}(t)$ and output $y(t)$ as follows: $H(y(t), V_{in}(t))$, see Fig. 6. According to this model, if $V_h = 0$, then the hysteresis will disappear, and if $R_a = \infty$ when $\|V_a\| < V_h$, then the creep will also disappear. Based on this proposed sandwich model and the equivalent circuitry as shown in Fig. 5, we can further derive the state model as follows:

$$\dot{V}_a(t) = -\Big(\frac{1}{R_a} + \frac{1}{R_o}\Big)\frac{V_a(t)}{C_a} - \frac{V_z(t)}{C_a R_o} + \frac{V_{in}(t)}{C_a R_o} \quad (1)$$

$$\dot{V}_z(t) = \frac{\dot{Q}_b}{C_z} + \frac{1}{C_z}\Big(-\frac{V_a(t)}{R_o} - \frac{V_z(t)}{R_o} + \frac{V_{in}(t)}{R_o}\Big), \quad (2)$$

where $Q_b = D_y F_z(t)$ is the "back electric charge force" (back-ecf) in a PEA, see [15]. According to [15] and the notation of Fig. 7, it is possible to write:

$$F_z(t) = M_p/3\ddot{x}(t) + D\dot{x}(t) + Kx(t) + K_x x(t). \quad (3)$$

K and D are the elasticity and the friction constant of the spring which is antagonist to the piezo effect and it is incorporated in the PEA. C_z is the total capacitance of the PEA and R_o is the contact resistance. For further details on this model see [15]. Considering the whole system described in Fig. 7 with the assumptions of incompressibility of the oil, the whole mechanical system can be represented by a spring mass structure as shown in the conceptual schema of Fig. 7. In this system the following notation is adopted: K_x is the elasticity constant factors of the PEA. In the technical literature, factor $D_x K_x = T_{em}$ is known with the name "transformer ratio" and states the most important characteristic of the electromechanical transducer. $M_p/3$ is, in our case, the moving mass of the piezo structure which is a fraction of whole piezo mass, M_{SK} is the sum of the mass of the piston with the oil and the moving actuator and M_v is the mass of the valve. It is possible to notice that the moving mass of the piezo structure is just a fraction of the whole piezo mass. The value of this fraction is given by the constructer of the piezo device and it is determined by experimental measurements. K_{SK} and D_{SK} are the characteristics of the antagonist spring to the mechanical servo valve, see Fig. 7. D_{oil} is the friction constant of the oil. Moreover, according to [15], motion $x_p(t)$ of diagram in Fig. 6 is

$$x_p(t) = D_x V_z(t). \quad (4)$$

According to the diagram of Fig. 5, it is possible to write as follows:

$$V_z = V_{in}(t) - R_0 i(t) - H(x_p(t), V_{in}(t)), \quad (5)$$

where R_0 is the connection resistance and $i(t)$ is the input current as shown in Fig. 5. $H(x_p(t), V_{in}(t))$ is the function which describes the hysteresis effect mentioned above and shown in the simulation of Fig. 6. Considering the whole system described in Fig. 7, the electrical and mechanical systems described in Figs. 5, 6 and 7 can be represented by the following mathematical expressions:

$$\frac{M_p}{3}\ddot{x}(t) + M_{SK}\ddot{x}_{SK}(t) + Kx(t) + D\dot{x}(t) + K_{SK}x_{SK}(t) + D_{SK}\dot{x}_{SK}(t) + D_{oil}\dot{x}_{SK}(t) + K_x\Big(x(t) - \Delta x_p(V_{in}(t))\Big) = 0, \quad (6)$$

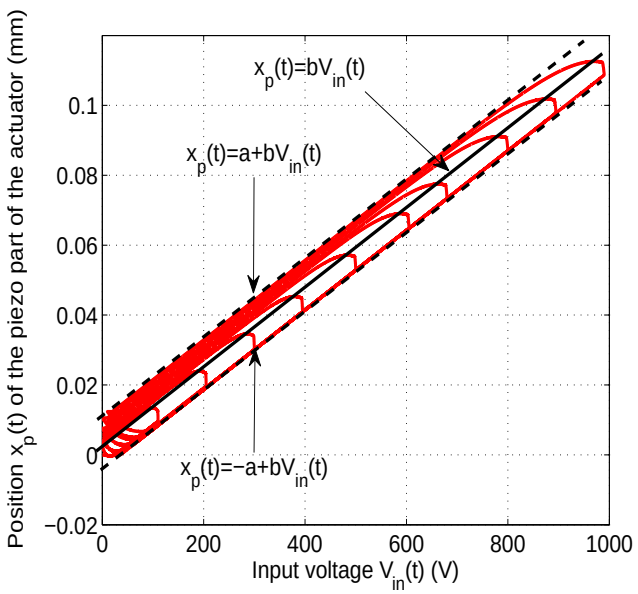

Fig. 6. Simulated Hysteresis curve of the piezo part of the actuator: $H(x_p(t), V_{in}(t))$

where $\Delta x_p(t)$ represents the interval function of $x_p(t)$ as shown in Fig. 6 which, according to equation (4), can be expressed as:

$$\Delta x_p(t) = D_x \Delta V_z(t). \tag{7}$$

Finally, using equations (5) and (7),

$$K_x \Delta x_p(t) = K_x D_x \big(V_{in}(t) - R_0 i(t) - H(\Delta x_p(t), V_{in}(t))\big), \tag{8}$$

which represents the interval force generated by the piezo device. Equation (6) can be expressed in the following way:

$$\frac{M_p}{3}\ddot{x}(t) + M_{SK}\ddot{x}_{SK}(t) + Kx(t) + D\dot{x}(t) + K_{SK}x_{SK}(t) + D_{SK}\dot{x}_{SK}(t) + D_{oil}\dot{x}_{SK}(t) + K_x x(t) = K_x \Delta x_p(V_{in}(t)). \tag{9}$$

It is to be noticed that the following relationship holds:

$$x_{SK}(t) = W x(t), \tag{10}$$

where W is the position ratio above defined and it states the incompressibility of the oil in the conic chamber. The following equation completes the dynamic of the considered system:

$$M_v \ddot{y}(t) + D_{oil}\dot{y}(t) = F\big(x_{SK}(t), y(t)\big) - F_d(t). \tag{11}$$

According to Fig. 7, $x(t)$ is the position of the piezo actuator, $x_{SK}(t)$ is the position of the mechanical servo actuator, $y(t)$ represents the position of the valve. Function $F(x_{SK}(t), y(t))$ represents the force exerted by the pump on surface S of the armature of the moving valve, see Fig 7. Moreover,

$$F(x_{SK}(t), y(t)) = (p_A(t) - p_B(t))S, \tag{12}$$

where $p_A(t)$ and $p_B(t)$ are the pressure in the two oil chambers separated by the armature of the valve. In [16] pressure $p_A(t)$ and $p_B(t)$ are nonlinear functions of the mechanical servo valve position $y(t)$. The linearization of this function at each desired position $y_d(t)$ will be considered later. $F_d(t)$ is the combustion back pressure in terms of force. According to Fig.

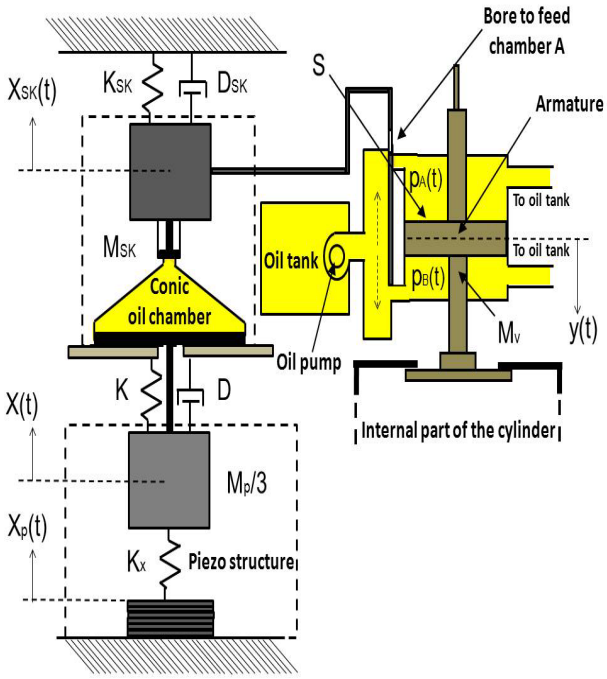

Fig. 7. Mass spring model of the whole actuator

6 in which an upper bound and a lower bound of the hysteresis curve are indicated, it is possible to write that:

$$\Delta x_p(V_{in}(t)) = [-a \quad a] + bV_{in}(t), \tag{13}$$

with $a \in \mathbb{R}$ and $b \in \mathbb{R}$ two positive constants are indicated. In particular,

$$\underline{\Delta} x_p(V_{in}(t)) = -a + bV_{in}(t), \tag{14}$$

and

$$\overline{\Delta} x_p(V_{in}(t)) = a + bV_{in}(t). \tag{15}$$

Considering this notation, the system represented in (6) can be split into the following two systems:

$a)$

$$\frac{M_p}{3}\ddot{x}(t) + M_{SK}\ddot{x}_{SK}(t) + Kx(t) + D\dot{x}(t) + K_{SK}x_{SK}(t) + D_{SK}\dot{x}_{SK}(t) + D_{oil}\dot{x}_{SK}(t) + K_x x(t) = \underline{\Delta} x_p(V_{in}(t)), \tag{16}$$

$b)$

$$\frac{M_p}{3}\ddot{x}(t) + M_{SK}\ddot{x}_{SK}(t) + Kx(t) + D\dot{x}(t) + K_{SK}x_{SK}(t) + D_{SK}\dot{x}_{SK}(t) + D_{oil}\dot{x}_{SK}(t) + K_x x(t) = \overline{\Delta} x_p(V_{in}(t)), \tag{17}$$

III. A SWITCHING CASCADE PID-PID CONTROLLER COMBINED WITH A FEEDFORWARD REGULATOR

Figure 8 shows the proposed control structure. It is possible to see how a feedforward structure is present in order to achieve a regulation around the desired trajectory. An internal PID structure and an external one complete the whole control scheme to guarantee the robustness. The feedforward control structure is based on the inversion of equations (16) and (17) together with equation (10). In the inversion of the whole model just the mechanical part of the model is considered. In fact, according to the real data which we have, the piezo and the hydraulic part of the model result to be more than 10 times faster than the mechanical part. According this considerations which result to be validated a posteriori with simulations, the feedforward controller consists of the digitalization of the following equation:

$$u_{feed}(t) = \frac{(\frac{M_p}{3} + M_{SK}W)\ddot{y}_d(t)}{K_x b} + \frac{\big(D + (D_{SK} + D_{oil})W\big)\dot{y}_d(t)}{K_x b} + \frac{(Ky + K_x + K_{SK})y_d(t) + K_x(-1)^q a}{K_x b}. \quad (18)$$

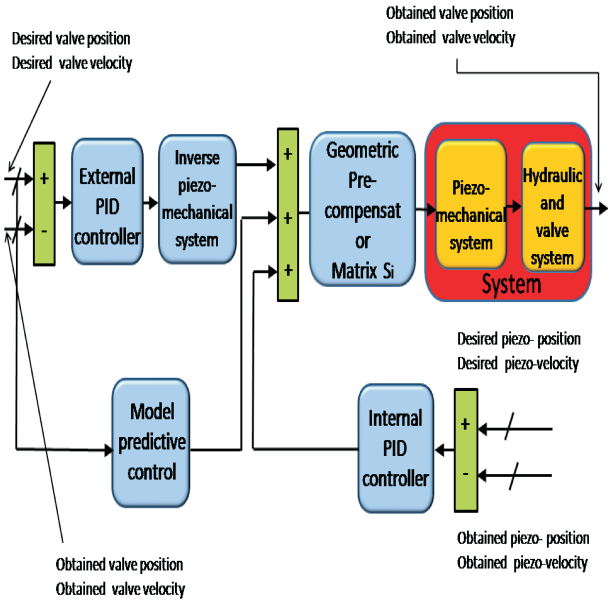

Fig. 8. Proposed control structure

A. A switching internal PID controller

As already mentioned, the PID control structure presented in this section is quite similar to the sliding control structure presented in [3]. In [4] an integral action is considered in a similar way as in this contribution in order to improve the controller performance in steady state (zero error). The proposed integral sliding mode control is derived using Lyapunov approach. Lyapunov approach is very used to derive control law also in industrial applications, e.g., [17]. Considering Figs. 5 and 7, if the dynamics shown in (16) and (17) are considered in a state space representation, then

$$\dot{x}_1(t) = x_2(t) \quad (19)$$

$$\dot{x}_2(t) = \frac{-Dx_2(t) - W(D_{SK} + D_{oil})x_2(t)}{\frac{M_p}{3} + M_{SK}W} + \frac{-(K + K_x + K_{SK}W)x_1(t)}{\frac{M_p}{3} + M_{SK}W} + \frac{3K_x b V_{in}(t) + (-1)^q a}{\frac{M_p}{3} + M_{SK}W} \quad (20)\text{–}(21)$$

where $q = 1, 2..$ The system represented in equations (19) and (21) can be represented as follows:

$$\begin{bmatrix} \dot{x}_1(t) \\ \dot{x}_2(t) \end{bmatrix} = \mathbf{f}(\mathbf{x}(t), H\big(y(t), V_{in}(t)\big)) + \mathbf{B}V_{in}(t), \quad (22)$$

where it is assumed that $V_{in}(t) = V_z(t)$,

$$\mathbf{f}(\mathbf{x}(t), H\big(y(t), V_{in}(t)\big)) = \begin{bmatrix} x_2(t) \\ \frac{-Dx_2(t) - (K + K_x + K_{SK}W)x_1(t)}{\frac{M_p}{3} + M_{SK}W} \end{bmatrix}, \quad (23)$$

and $\mathbf{B} = \begin{bmatrix} 0 \\ \frac{3K_x b + (-1)^q a}{\frac{M_p}{3} + M_{SK}W} \end{bmatrix}$. The following PID controller is defined:

$$K(t) = \mathbf{G}\big(\mathbf{x}_d(t) - \mathbf{x}(t)\big), \quad (24)$$

where $\mathbf{G} = \begin{bmatrix} P_i & D_i \end{bmatrix}$, and $\mathbf{x}_d(t)$ represents the vector of the desired piezo trajectories. Equation (24) becomes as follows:

$$K_i(t) = \begin{bmatrix} P_i & D_i \end{bmatrix} \begin{bmatrix} x_{1d}(t) - x_1(t) \\ x_{2d}(t) - x_2(t) \end{bmatrix} + I_i \int (x_{1d}(t) - x_1(t))dt, \quad (25)$$

thus

$$K_i(t) = P_i\big(x_{1d}(t) - x_1(t)\big) + D_i\big(x_{2d}(t) - x_2(t)\big) + I_i \int (x_{1d}(t) - x_1(t))dt, \quad (26)$$

P_i and D_i are internal P and internal D parameters of the PID controller. If the following Lyapunov function is defined:

$$V(K_i) = \frac{K_i^2(t)}{2}, \quad (27)$$

then it follows that:

$$\dot{V}(K_i) = K_i(t)\dot{K}_i(t). \quad (28)$$

In order to find the stability of the solution $s(t) = 0$, it is possible to choose the following function:

$$\dot{V}(K_i) = -\eta(t){K_i}^2(t), \quad (29)$$

with $\eta > 0$. Comparing (28) with (29), the following relationship is obtained:

$$K_i(t)\dot{K}_i(t) = -\eta K_i^2(t), \tag{30}$$

and finally

$$K_i(t)\big(\dot{K}_i(t) + \eta K_i(t)\big) = 0. \tag{31}$$

The no-trivial solution follows from the condition

$$\dot{K}_i(t) + \eta K_i(t) = 0. \tag{32}$$

From (24) it follows:

$$\dot{K}_i(t) = \mathbf{G}\big(\dot{\mathbf{x}}_d(t) - \dot{\mathbf{x}}(t)\big) + I_i(x_{1d}(t) - x_1(t)) = \mathbf{G}\dot{\mathbf{x}}_d(t) - \mathbf{G}\dot{\mathbf{x}}(t) + I_i(x_{1d}(t) - x_1(t)). \tag{33}$$

The main idea is to find a $u_{eq}(t)$, an equivalent input, and after that a $V_{in}(t)$, such that $\dot{\mathbf{x}}(t) = \dot{\mathbf{x}}_d(t)$. For that, from (22) it follows that:

$$\dot{\mathbf{x}}(t) = \dot{\mathbf{x}}_d(t) = \mathbf{f}(x_d(t), H) + \mathbf{B}V_{in}(t), \tag{34}$$

and from (33) the following relationship is obtained:

$$\dot{K}_i(t) = \mathbf{G}\dot{\mathbf{x}}_d(t) - \mathbf{G}\mathbf{f}(x_d(t), H) - \mathbf{G}\mathbf{B}V_{in}(t) = \mathbf{G}\mathbf{B}\big(u_{eq}(t) - V_{in}(t)\big) + I_i(x_{1d}(t) - x_1(t)), \tag{35}$$

where $u_{eq}(t)$ is the equivalent input which, in our case, assumes the following expression:

$$u_{eq}(t) = \big(\mathbf{G}\mathbf{B}\big)^{-1}\mathbf{G}\Big(\dot{\mathbf{x}}_d(t) - \mathbf{f}(x_d(t), H)\Big). \tag{36}$$

After inserting (35) in (32) the following relationship is obtained:

$$\mathbf{G}\mathbf{B}\big(u_{eq}(t) - V_{in}(t)\big) + \eta K_i(t) = 0, \tag{37}$$

and in particular

$$V_{in}(t) = u_{eq}(t) + \big(\mathbf{G}\mathbf{B}\big)^{-1}\eta K_i(t). \tag{38}$$

Normally, it is a difficult job to calculate $u_{eq}(t)$. If equation (35) is rewritten in a discrete form using Euler approximation, then it follows:

$$\frac{K_i((k+1)T_s) - K_i(kT_s)}{T_s} = \mathbf{G}\mathbf{B}\big(u_{eq}(kT_s) - V_{in}(kT_s)\big). \tag{39}$$

If equation (38) is also rewritten in a discrete form, then:

$$V_{in}(kT_s) = u_{eq}(kT_s) + \big(\mathbf{G}\mathbf{B}\big)^{-1}\eta K_i(kT_s). \tag{40}$$

Equation (39) can be also rewritten as:

$$u_{eq}(kT_s) = V_{in}(kT_s) + \big(\mathbf{G}\mathbf{B}\big)^{-1}\frac{K_i((k+1)T_s) - K_i(kT_s)}{T_s}. \tag{41}$$

Equation (41) can be estimated to one-step backward in the following way:

$$u_{eq}((k-1)T_s) = V_{in}((k-1)T_s) + \big(\mathbf{G}\mathbf{B}\big)^{-1}\frac{K_i(kT_s) - K_i((k-1)T_s)}{T_s}. \tag{42}$$

Because of function $u_{eq}(t)$ being a continuous one, we can write:

$$u_{eq}(kT_s) \approx u_{eq}((k-1)T_s). \tag{43}$$

Considering equation (43), then equation (42) becomes:

$$u_{eq}(kT_s) = V_{in}((k-1)T_s) + \big(\mathbf{G}\mathbf{B}\big)^{-1}\frac{K_i(kT_s) - K_i((k-1)T_s)}{T_s}. \tag{44}$$

Inserting (44) into (40):

$$V_{in}(kT_s) = V_{in}((k-1)T_s) + \big(\mathbf{G}\mathbf{B}\big)^{-1}\Big(\eta K_i(kT_s) + \frac{K_i(kT_s) - K_i((k-1)T_s)}{T_s}\Big), \tag{45}$$

and finally:

$$V_{in}(kT_s) = V_{in}((k-1)T_s) + \big(\mathbf{G}\mathbf{B}T_s\big)^{-1}\Big(\eta T_s K_i(kT_s) + K_i(kT_s) - K_i((k-1)T_s)\Big). \tag{46}$$

Through matrix $\mathbf{B}$ the control law is a switching one.

B. A switching external PID controller

If the following external PID is defined:

$$s_e(t) = \begin{bmatrix} P_e & D_e \end{bmatrix}\begin{bmatrix} x_{1vd}(t) - x_{1v}(t) \\ x_{2vd}(t) - x_{2v}(t) \end{bmatrix} + I_e\int(x_{1vd}(t) - x_{1v}(t))dt, \tag{47}$$

where $\mathbf{x}_{vd}(t)$ represents the vector of the desired valve trajectories. Then after similar calculation the following PID structure is calculated:

$$V_{in}(kT_s) = V_{in}((k-1)T_s) + \big(\mathbf{L}\mathbf{H}T_s\big)^{-1}\Big(\eta T_s K_i(kT_s) + K_e(kT_s) - K_e((k-1)T_s)\Big). \tag{48}$$

The following notation is used: $\mathbf{L} = \begin{bmatrix} P_e & D_e \end{bmatrix}$ and

$$\mathbf{H} = \begin{bmatrix} 0 \\ -F(x_{SK_d}(t)y_d(k))/M_v \end{bmatrix}, \tag{49}$$

where $c_{x_{SK_d}(k)} \in \mathbb{R}$ and $c_{y_d(k)} \in \mathbb{R}$ are the constants which come from the linearization of $F(x_{SK}(t), y(t))$ at each t-time.

IV. A Geometric pre-compensator to speed up the controlled dynamics

Assuming that state of the system as follows, then:

$$\mathbf{x}_f(t) = \begin{bmatrix} x(t) & \dot{x}(t) & y(t) & \dot{y}(t) \end{bmatrix}^T, \tag{50}$$

and considering equation (11), and (14) with (15) combined with (16) and (17), the following matrices for the representation of the system are obtained:

$$\mathbf{A}_k = \begin{bmatrix} 0 & 1 & 0 & 0 \\ -\frac{(K_x+K+K_{SK}W)}{\frac{M_p}{3}+M_{SK}W} & -\frac{(D+(D_{SK}+D_{oil})W)}{\frac{M_p}{3}+M_{SK}W} & 0 & 0 \\ 0 & 0 & 0 & 1 \\ \frac{c_x(k)}{M_v} & 0 & \frac{c_y(k)}{M_v} & -\frac{D_{oil}}{M_v} \end{bmatrix}, \tag{51}$$

where $c_x(k) \in \mathbb{R}$ and $c_y(k) \in \mathbb{R}$ are elements which come from the linearization of $F(x_{SK}(t), y(t))$. Matrix $\mathbf{A}$ represents, as written above, the Jacobian matrix of the system.

$$\mathbf{B}_k = \begin{bmatrix} 0 \\ \frac{3K_x b}{M_p+3M_{SK}W} \\ 0 \\ 0 \end{bmatrix}, \quad \mathbf{E}_k = \begin{bmatrix} 0 & 0 & 0 & 0 \\ 0 & \frac{3K_x a}{M_p+3M_{SK}W} & 0 & 0 \\ 0 & 0 & 0 & 0 \\ 0 & 0 & 0 & -\frac{1}{M_v} \end{bmatrix},$$

$$\mathbf{d}(k) = \begin{bmatrix} 0 \\ T_r(k) \\ 0 \\ -F(x_{SK_d}(k) y_d(k)) - F_L(k) \end{bmatrix}. \quad (52)$$

$x_{SK_d}(k)$ and $y_d(k)$ are the desired trajectories of the moving mass and the desired output respectively at each k-time. Term $F(x_{SK_d}(k), y_d(k))$ comes from the linearization of $F(x_{SK}(t), y(t))$ at the desired trajectories.

$$T_r = -sign(V_{in}(k) - V_{in}(k-1) - V_h(k)), \quad (53)$$

where $V_h(k)$ is a suitable threshold voltage as proposed for the construction of the hysteresis in [15]. Term T_r states the switching nature of the model.

A. Solving a linear position MPC optimization problem

Considering the models described in (11), (16) and (17) in which Euler discretization is considered with $k = nt_s$, $n \in \mathbb{N}$, where T_s is the sampling time, if $y(t)$ is assumed to be the controlled output, then the following system is obtained:

$$\begin{aligned} \mathbf{x}_f(k+1) &= \mathbf{A}_k \mathbf{x}_f(k) + \mathbf{B}_k V_{in}(k) + \mathbf{E}_k \mathbf{d}(k) \\ y(k) &= \mathbf{H}_k \mathbf{x}_f(k), \end{aligned} \quad (54)$$

where matrix $\mathbf{H}_k = [0 \quad 0 \quad 1 \quad 0]$ is the output matrix which determines the position of the valve according to the system in (6) and (11). Matrix $\mathbf{A}_k$ represents the digitalization of the system described in (6) and (11). A particular attention should be paid to matrices $\mathbf{B}_k$, $\mathbf{E}_k$ and $\mathbf{d}_k$ which take the switching aspect in the represented system into account. In the MPC approach just two samples are considered:

$$\begin{aligned} y(k+1/k) = \mathbf{H}_k \mathbf{A}_k \mathbf{x}_f(k) + \mathbf{H}_k \mathbf{B}_k u_{mpc}(k) \\ + \mathbf{H}_k \mathbf{E}_k \mathbf{d}(k) \end{aligned} \quad (55)$$

$$\begin{aligned} y(k+2/k) = \mathbf{H}_k \mathbf{A}_k^2 \mathbf{x}_f(k) + \mathbf{H}_k \mathbf{A}_k \mathbf{B}_k u_{mpc}(k) \\ + \mathbf{H}_k \mathbf{B}_k u_{mpc}(k+1) + \mathbf{H}_k \mathbf{A}_k \mathbf{E}_k \mathbf{d}(k) + \mathbf{H}_k \mathbf{E}_k \mathbf{d}(k). \end{aligned} \quad (56)$$

Equations (55) and (56) can be vectorially expressed as:

$$\mathbf{Y}(k) = \mathbf{G}_p \mathbf{x}_f(k) + \mathbf{F}_{1p}(k) \mathbf{U}_{mpc}(k) + \mathbf{F}_{3p} \mathbf{d}(k). \quad (57)$$

If the following performance criterion is assumed,

$$\begin{aligned} J = \frac{1}{2} \sum_{j=1}^{N} \Big(y_d(k+j) - y(k+j) \Big)^{\mathrm{T}} \mathbf{Q}_p \Big(y_d(k+j)) \\ - y(k+j) \Big) + \frac{1}{2} \sum_{j=1}^{N} \Big(u_{mpc}(k+j) \Big)^{\mathrm{T}} \mathbf{R}_p u_{mpc}(k+j), \end{aligned} \quad (58)$$

where $y_d(k+j)$, $j = 1, 2, \ldots, N$ is the position reference trajectory (desired trajectory) and N the number of samples of the prediction horizon, and $\mathbf{Q}_p$ and $\mathbf{R}_p$ are non-negative definite matrices, then the solution minimizing performance index (58) may be obtained by solving

$$\frac{\partial J}{\partial u_{mpc}(k)} = 0. \quad (59)$$

If only two steps for the prediction horizon are considered, then:

$$\mathbf{F}_{1p} = \begin{bmatrix} \mathbf{H}_k \mathbf{B}_k & \mathbf{0} \\ \mathbf{H}_k (\mathbf{A}_k \mathbf{B}_k + \mathbf{B}_k) & \mathbf{H}_k \mathbf{B}_k \end{bmatrix}, \quad \mathbf{G}_p = \begin{bmatrix} \mathbf{H}_k \mathbf{A}_k \\ \mathbf{H}_k \mathbf{A}_k^2 \end{bmatrix},$$

$$\mathbf{F}_{3p} = \begin{bmatrix} \mathbf{H}_k \mathbf{E}_k & \mathbf{0} \\ \mathbf{H}_k (\mathbf{A}_k \mathbf{E}_k + \mathbf{E}_k) & \mathbf{H}_k \mathbf{E}_k \end{bmatrix}. \quad (60)$$

A direct off-line computation may be obtained explicitly as:

$$\begin{aligned} u_{mpc} = (\mathbf{F}_{1p}^{\mathrm{T}} \mathbf{Q}_p \mathbf{F}_{1p} + \mathbf{R}_p)^{-1} \Big(\mathbf{F}_{1p}^{\mathrm{T}} \mathbf{Q}_p \\ \times \big(\mathbf{Y}_{d_p}(k) - \mathbf{G}_p \mathbf{x}(k) - \mathbf{F}_{3p} \mathbf{d}(k) \big) \Big), \end{aligned} \quad (61)$$

where $\mathbf{Y}_{d_p}(k)$ and $\mathbf{Y}_p(k)$ are the desired output column vector and the measured or observed output vector. For further details see [18]. In order to speed up the dynamics of the actuator without using strong actions of the regulators which can generate large oscillations and thus tracking errors, a geometric pre-compensator is proposed. The idea is to select an eigenvector of $\mathbf{G}_{1p}$ which represents the matrix of the predicted dynamics of the whole actuator. This eigenvector must be included into the intersection between $\mathsf{im}\mathbf{F}_{1p}$ and between the set of the eigenvectors of matrix $\mathbf{G}_{1p}$. Once the eigenvector which corresponds to the biggest absolute value of the eigenvalue is chosen, according to the meaning of the eigenvalues and eigenvectors, then it is possible to control the system along the direction of this eigenvector to obtain the fastest dynamics. The advantage here is that this dynamics can be reached just using a pre-compesator which should select the eigenvector of the system. The feedback parts of the controllers are devoted to make the whole control system robust. If a matrix $\mathbf{I}_\lambda$ is considered, and

$$\mathsf{im}\mathbf{I}_\lambda = \{\mathsf{im}\mathbf{F}_{1p} \cap \mathsf{im}\mathbf{V}\}, \quad (62)$$

where $\mathbf{V}$ represents the matrix containing all eigenvectors of matrix $\mathbf{G}_p$, then subspace $\mathsf{im}\mathbf{I}_\lambda$ represents the intersection subspace between the matrix of the eigenvectors and the input matrix $\mathbf{F}_{1p}$. Considering $\mathbf{I}_{\lambda_{max}}$ which represents the eigenvector of the set defined in (62) which corresponds to the maximal eigenvalue, then we are looking for an input partition matrix $\mathbf{S}_i$ such that, for the dynamic triples

$$(\mathbf{I}_{\lambda_{max}}, \mathbf{G}_p, \mathbf{F}_{1p}\mathbf{S}_i), \quad (63)$$

the requirements

$$\mathcal{R}_{I_i} = \mathsf{min}\mathcal{I}(\mathbf{G}_p, \mathbf{F}_{1p}\mathbf{S}_i) \subseteq \mathsf{im}\mathbf{I}_{\lambda_{max}} \quad (64)$$

can be achieved.

About the calculation of the preselecting matrix $\mathbf{S}_i$, if $\mathsf{im}\mathbf{F}_{1p} \cap \mathsf{im}\mathbf{V} \neq 0$, then:

$$\mathbf{S}_i = (\mathbf{F}_{1p}^T \mathbf{F}_{1p})^{-1} \mathbf{F}_{1p}^T \mathbf{I}_{\lambda_{max}}. \quad (65)$$

V. Simulation results

The control law of equation (46) is tested using the model described in section II. Figure 9 shows the final results concerning the tracking of a desired position of an exhaust valve with 8000 rpm. Figure 10 shows the final results concerning the tracking of a desired velocity of an exhaust valve with 8000 rpm. Figure 11 shows the profile of the simulated force on the piezo part of the proposed actuator. But, the force acting directly on the valve at the opening time has a peak value equal to 700 N circa and it is reduced to a few Newtons acting on the piezo part thanks to the decoupling structure of the hybrid actuator. This is one of the greatest advantages of these hybrid actuators. The model of such kind of a disturbance is obtained as an exponent function of the position of the valve. Figure 12 shows the pressure profile of pressure $p_A(t)$ and $p_B(t)$ of the oil chambers of Fig. 7.

The digital controller is set to work with a sampling time equal to 20×10^{-6} s, according to the specifications of the Digital Signal Processor which we are intended to test the system with.

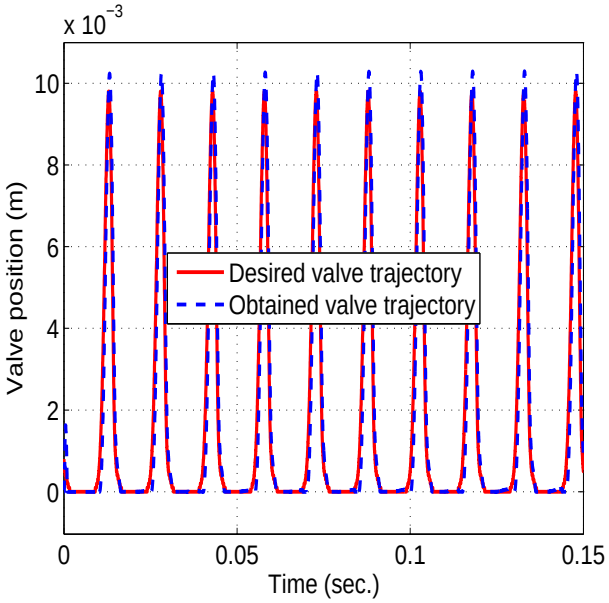

Fig. 9. Desired and obtained valve positions corresponding to 8000 rpm

Remark 1: It is to remark that, equation (46) states that the control law does not depend on the dynamics of the system model. The control law depends for the internal PID controller just on the moving mass and on product $K_x D_x$ (transformer ratio). All these parameters are always well known in a piezoelectric actuator. Product $K_x D_x$ depends on the temperature, the piezoelectric actuator is equipped with a temperature sensor which activates an air cooling system. Concerning external PID controller, the control law depends on the moving mass and on the pressures of the two oil chambers, and on the valve surface.

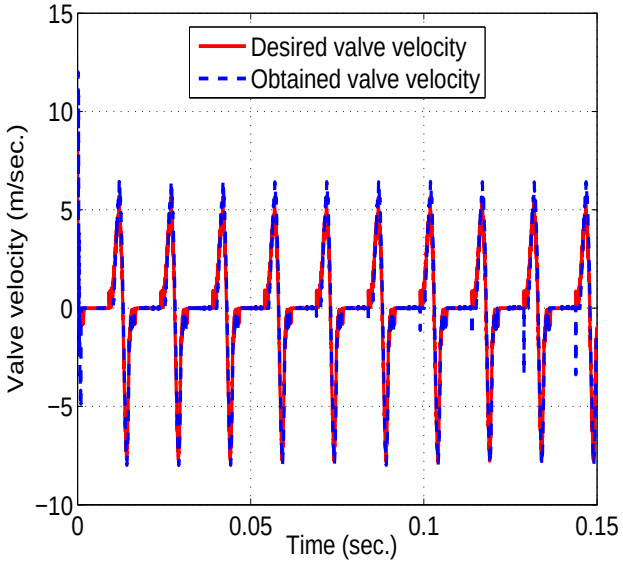

Fig. 10. Desired and obtained valve velocity (8000 rpm)

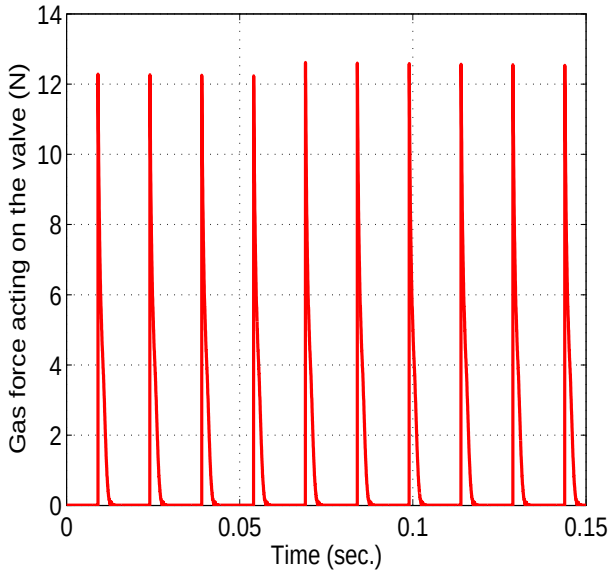

Fig. 11. Force of the internal combustion considering 8000 rpm

VI. Conclusions and future work

A. Conclusions

This paper deals with a hybrid actuator composed by a piezo part and a hydraulic one and its control structure for camless engine motor applications. The idea is to use the advantages of both, the high precision of the piezo part and the force of the hydraulic one. In the control problem nonlinearities such as hysteresis, saturations, and creep are taken into account. The proposed control scheme integrates PID controleer together with a feedforward controller and an MPC structure using a geometric structure to speed up the dynamic response. Simulations with real data of motor and of a piezo actuator are shown.

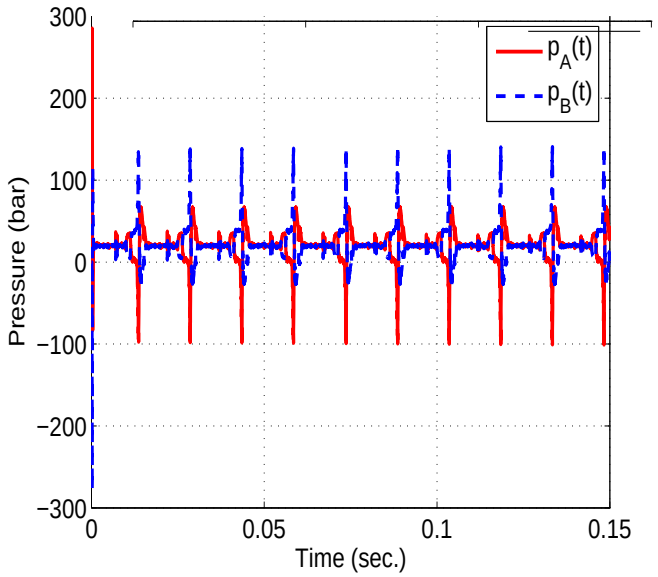

Fig. 12. Pressure $p_A(t)$ and $p_B(t)$ of the oil chambers considering 8000 rpm

B. Future work

Future contributions include an adaptive PID-PID control structure and measurements on an experimental setup. Some refined models of the whole structure are already under consideration. In particular, in the presented paper it is assumed that the oil of the hydraulic part is incompressible. This assumption should be removed and the pressure of the oil should be considered as a further state variable which the system can be described with. Moreover, advanced future contributions should consider sensorless control structure as proposed in [19] and in [20] for an electromechanical actuator.

REFERENCES

[1] D. Liviu, C. Jenica, L. Mihai, and T. Alexandru. Mathematical models and numerical simulations for electro-hydrostatic servo-actuators. *INTERNATIONAL JOURNAL OF CIRCUITS, SYSTEMS AND SIGNAL PROCESSING*, 2(4):229–238, 2008.

[2] S. Koprda, Z. Balogh, and M. Turcani. Modeling and comparison of fuzzy PID controller with psd regulation in the discrete systems. *INTERNATIONAL JOURNAL OF CIRCUITS, SYSTEMS AND SIGNAL PROCESSING*, 5(5):496–504, 2011.

[3] J. Lee, D. Lee, and S. Won. Precise tracking control of piezo actuator using sliding mode control with feedforward compensation. In *Proceedings of SICE Annual Conference 2010*, pages 1244–1249, Taipei, 18^{th}-21^{st} August 2010.

[4] M.Y Ali. Experimental set up verification of servo dc motor position control based on integral sliding mode approach. *WSEAS TRANSACTIONS on SYSTEMS and CONTROL*, 7(3):87–96, 2013.

[5] S.A.E.M. Ardjoun, M. Abid, A.G. Aissaoui, and A. Naceri. A robust fuzzy sliding mode control applied to the double fed induction machine. *INTERNATIONAL JOURNAL OF CIRCUITS, SYSTEMS AND SIGNAL PROCESSING*, 5(4):315–321, 2011.

[6] S.A. Al-Samarraie. Invariant sets in sliding mode control theory with application to servo actuator system with friction. *WSEAS TRANSACTIONS on SYSTEMS and CONTROL*, 8(2):33–45, 2013.

[7] Xiao Lv, Yue Sun, Zhi-Hui Wang, and Chun-Sen Tang. Development of current-fed icpt system with quasi sliding mode control. *WSEAS TRANSACTIONS on SYSTEMS and CONTROL*, 6(1):1–15, 2012.

[8] P. Mercorelli, S. Liu, and K. Lehmann. Robust flatness based control of an electromagnetic linear actuator using adaptive PID controller. In *Proceeding of the 42^{nd} IEEE Conference on Decision and Control*, pages 3790–3795, Hyatt Regency Maui, Hawaii, (USA), 9^{th}-12^{th} December 2003.

[9] P. Mercorelli and N. Werner. An adaptive Lyapunovs internal PID regulator in automotive applications. In *WSEAS Recent Advances in Systems, Control Signal Processing and Informatics, Proceedings of the 2013 International Conference on Systems, Control, Signal Processing and Informatics (SCSI 2013)*, pages 141–146, Rhodes, July 2013.

[10] P. Mercorelli, N. Werner, U. Becker, and H. Harndorf. Model predictive control of transistor pulse converter for feeding electromagnetic valve actuator with energy storage. In *Proceedings of SSD 12. 9th IEEE International Conference on Systems, Signals and Devices, 2012*, pages 1–6, Chemnitz, March 2012.

[11] Po-Kwang Chang Jium-Ming Lin. Eliminating hysteresis effect of force actuator in a spm. *WSEAS TRANSACTIONS on CIRCUITS and SYSTEMS*, 11(11):351–350, 2010.

[12] P. Mercorelli. A switching Kalman filter for sensorless control of a hybrid hydraulic piezo actuator using mpc for camless internal combustion engines. In *Proceedings of the 2012 IEEE International Conference on Control Applications*, pages 980–985, Dubrovnik, 3-5 October 2012.

[13] G. Basile and G. Marro. *Controlled and conditioned invariants in linear system theory*. Prentice Hall, New Jersey-USA, 1992.

[14] H.J.M.T.A. Adriaens, W.L. de Koning, and R. Banning. Modeling piezoelectric actuators. *IEEE/ASME Transactions on Mechatronics*, 5(4):331–341, 2000.

[15] Y.-C. Yu and M.-K. Lee. A dynamic nonlinearity model for a piezo-actuated positioning system. In *Proceedings of the 2005 IEEE International Conference on Mechatronics, ICM 2005*, pages 28–33, Taipei, 10^{th}-12^{th} July 2005.

[16] H. Murrenhoff. *Servohydraulik*. Shaker Verlag, Aachen, 2002.

[17] Prechanon Kumkratug. Statcom control strategy based on Lyapunov energy function and fuzzy logic control for improving transient stability of multimachine power system. *WSEAS TRANSACTIONS on CIRCUITS and SYSTEMS*, 11(5):159–168, 2012.

[18] S. Huang, T.K. Kiong, and T.H. Lee. *Applied Predictive Control*. Springer-Verlag London, Printed in Great Britain, 2002.

[19] P. Mercorelli. A hysteresis hybrid extended Kalman filter as an observer for sensorless valve control in camless internal combustion engines. *IEEE Transactions on Industry Applications*, 48(6):1940–1949, 2012.

[20] P. Mercorelli. A two-stage augmented extended Kalman filter as an observer for sensorless valve control in camless internal combustion engines. *IEEE Transactions on Industrial Electronics*, 59(11):4236–4247, 2012.